International Journal of Environment and Geoinformatics 11(3):030-048(2024)

Research Article

Enhancing Burned Area Mapping Accuracy: Integrating Multi-temporal PCA with NDVI Analysis

Souad Ghouzlane[1]*, Okan Fıstıkoğlu

Geographic Information Systems, Graduate School of Applied and Natural Sciences, Dokuz Eylul University, Izmir, Türkiye

* Corresponding author: S. Ghouzlane
E-mail: souad.ghouzlane@ogr.deu.edu.tr

Received: 15.07.2024
Accepted: 03.09.2024

How to cite: Ghouzlane and Fıstıkoğlu (2024). Enhanced Burned Area Mapping Accuracy*: Integrating Multi-temporal PCA with NDVI Analysis. International Journal of Environment and Geoinformatics (IJEGEO)*, 11(3): 030-048. doi. 10.30897/ijegeo.1516280

Abstract

Forested lands on the west coast of Türkiye, with their similarity to Mediterranean forests, are often found to be highly susceptible to wildfires, necessitating the development of a forest management program to refine and quantify forest fires and their impacts on the environment. In light of this fact, a multi-temporal approach combining Principal Component Analysis (PCA) and Normalized Difference Vegetation Index (NDVI) analysis derived from Sentinel-2 imagery is suggested in the current study. Through PCA of carefully selected bands of Sentinel-2, we attempt to capture both recent and historic fire impacts. It was found that the first two principal components (PC1 and PC2) predominantly describe landscape characteristics, while the third and fourth components (PC3 and PC4) have high abilities in detecting burn scars. It is worth noting that an increase in the ability to detect burn scars was observed with the inclusion of NDVI and its difference in time ($\Delta NDVI$) within the PCA process. A high effectiveness level in distinguishing burnt areas from unburnt landscapes was presented by the multi-temporal PCA approach, particularly with $\Delta NDVI$ integration. PC2 and PC3, especially with $\Delta NDVI$ integration, were found to be strong indicative factors of burnt areas. In the classification result, accuracies of different years of fire events differed, and a high accuracy of 98.76% was found in the last fire event year of 2019. However, slight underestimation and overestimation were also observed in older fire scars. Mean accuracy, on average, for the PCA-$\Delta NDVI$ method was found to be higher than that of the Maximum Likelihood Classification (MLC) method. Furthermore, significant vegetation losses by fire, particularly by the 2019 fire incident, were realized through NDVI assessment. Although it worked well in recent fire scars, overestimating the extent in the case of burned areas from previous years was observed. The results of this work highlight the potential of integrating multi-temporal PCA with NDVI for mapping burned areas at various scales in fire-prone ecosystems in western Türkiye. This approach contributes to the development of more effective forest management and assessment strategies following fires in these ecosystems. Moreover, the approach is suggested to be one of the strong tools for monitoring fire-induced damages across many time scales toward better understanding and management of long-term impacts caused by forest fires in the region.

Keywords: Forest fires, Burned areas, PCA, NDVI

Introduction

In recent years, the frequency and intensity of fires in the natural ecosystems have increased significantly. According to the European Forest Fire Information System (EFFIS), the average annual burned area in the Mediterranean countries has more than doubled in the last decade compared to the 1980s" (San-Miguel-Ayanz et al., 2020). According to data from the General Directorate of Forestry of Türkiye, huge waves have been present in case numbers and acres affected between 2008 and 2022 all over the country (General Directorate of Forestry, 2022) While the number of fires noted in 2008 was 2,135 that had increased to 3,399 by 2020. However, 2021 was absolutely the worst, with 2,793 forest fires counted. These differences drastically changed the affected areas from 3,117 hectares in 2021. Interestingly, this is not directly proportional to the affected areas most of the time. For example, whereas 2020 had more fires (3,399) compared to 2008, which had 2,135, the affected area stood at 29,749 ha in 2008, compared with 20,971 ha in 2020 (General Directorate of Forestry, 2022). This indicates that the relationship is not monotonic, reflecting the complexity of forest fires and their impacts. The significant variation in the number of fire occurrences and affected areas underscores the critical need for advanced, reliable methods capable of assessing forest fire impacts. This will be extremely helpful in understanding the fire pattern and developing better management strategies to reduce the ecological and economic impacts of forest fires in the region.

While remote-sensing techniques have proven to be of great value in burned area assessment, several existing methods are faced with quite a few challenges concerning the accurate delineation of burn scars in landscapes of complex nature. Traditional approaches might struggle through spectral confusion between the burned areas and other dark surface features, or in depicting the full extent of partially burned regions (Lentile et al., 2006). Besides, the recovery rate can be different for various vegetation's, and, according to Veraverbeke et al. (2010), it may limit the effectiveness of single-date post-fire imagery. The above limits are overcome in this paper by combining multi-temporal Principal Component Analysis with vegetation indices, hence possibly offering enhanced

accuracy in the detection of burn scars and extent estimation. Accurate burned area mapping bears great importance, not only for the purpose of quantifying the impacts brought about by fire but also to inform appropriate restoration efforts in forests, enhance resource management efficiency in case of a fire occurrence, and attain a better understanding of fire ecology dynamics (Chuvieco et al., 2019). This research improves the accuracy of burned area estimates, hence helping to support more robust forest management practices and evidence-based decision-making in fire-prone areas.

Remote sensing techniques have been very useful for fire-prone landscapes, allowing large-area monitoring and enforcing the consistent availability of data, making it possible to be covered under a wide range of wavelengths. These techniques, widely applied in land use change detection and burned area evaluation, include image classification (Cihlar et al., 1998; Khorrami et al., 2019; Sunar Erbek et al., 2004; Tuia et al., 2011), dimensional transformations (Carper et al., 1990; Choi, 2006; Huang et al., 2022; Leung et al., 2014; Lu et al., 2011), spectral indices, and machine learning algorithms.

Principal Component Analysis (PCA) is known as one of the main techniques, probably the most versatile and useful in remote sensing and in pattern recognition. PCA is a statistical technique to discover the principal structure of image data sets (Wintz, 1973). It has been applied to digital image enhancement, detecting temporal changes in digital images, and analyzing seasonal variations in land cover types (Walsh et al., 1990; Byrne et al., 1980; Townshend et al., 1985). In essence, PCA involves a combination of variables correlated to obtain new, uncorrelated combinations; each principal component has a successively smaller variance than the previous one. What is more, this very property makes PCA especially useful and effective when original variables happen to be highly correlated, because in that instance, the first few principal components may capture most of the total variance.

Therefore, in multi-temporal data change detection analysis for burned area mapping, PCA is especially efficient at highlighting the differences related to burn scars by analyzing the variation of the data before and after a fire event. Although a conventional way of mapping these areas is mostly based on detailed field surveys and aerial photography, PCA provides a faster technique to process satellite data for change detection purposes without heavy fieldwork and therefore can give timely information about the burned area.

The current study makes use of remote sensing indices, such as the Normalized Difference Vegetation Index in conjunction with multi-temporal PCA for optimizing the estimated variance of the datasets. During this process, areas without substantial changes show a high correlation and areas with large changes have lower correlation. This approach allows one to determine which combination among the bands is the best for a selective band PCA and to evaluate the accuracy of the resulting map using official data provided by the National Forest Service.

In this regard, three major fire incidents that occurred in two districts of İzmir Province, Seferihisar and Menderes, within the period between 2016 and 2019, are focused. The largest fire was that of 2019, which burned an area of about 5000 hectares of forestland, while two other fires previously occurred in 2016 burning about 500 ha and in 2017 burning 986 ha (General Directorate of Forestry, 2020). The timeline for fire events and the corresponding Sentinel-2 image acquisition dates is summarized in Table 1.

Table 1.Fire Events and Sentinel-2 images Acquisition Timeline

Fire Event	Initial Date	Final Date	Acquisition Time
Fire 2016	8/3/2016	8/3/2016	9/15/2016
Fire 2017	7/1/2017	7/3/2017	8/26/2017
Fire 2019	8/18/2019	8/20/2019	9/15/2019

In the present study, Sentinel-2 imagery was used with its native spatial resolution of 10 meters for key bands, a revisit time of 5 days at the equator, and free-of-cost availability. Such characteristics make Sentinel-2 perfectly suitable for monitoring dynamic events like forest fires and subsequent vegetation recovery. Table 1 The main objectives of this research can be viewed three-fold:

1. Mapping the spatial extent of burnt areas due to three different fire incidents using an integrated multi-temporal Principal Component Analysis and Normalized Difference Vegetation Index analysis.
2. Visualizing the affected regions to assess the damages caused by the fires, emphasizing the importance of accurately mapping these areas.
3. Determining the accuracy of detection methodologies for burned areas to ensure the scientific validity and reliability of the findings.

The burned area maps were validated against official fire perimeter data from the Turkish General Directorate of Forestry and MODIS burned area products. The accuracy of the multi-temporal PCA-based $\Delta NDVI$ was further checked by the obtained results using the Maximum Likelihood Classification method. Description of the patterns of spatial spreading and trends in intensity observed for the fires over the area studied provide insight into how forest fires behave in the region. The following are particularly important objectives to achieve an improved understanding of fire behavior in Western Türkiye's fire-prone ecosystems and to evaluate how effective remote sensing-based approaches would be, more specifically, by using the integration of multi-temporal PCA and $\Delta NDVI$ for fire detection and analysis.

Materials and Methods

Study Area Description

The study area includes the Seferihisar and Menderes districts in the İzmir Province, a coastline province of

Western Türkiye. It is approximately located between 26°45′–27°20′ east longitudes and 37°60′–38°20′ north latitudes. It covers an area of approximately 1168 km2, with a perimeter of about 256 km. From a geological perspective, it is a heterogeneous region with various rock types, particularly limestones and marbles, which have important industrial uses. This Mediterranean climate; with hot, dry summers and mild rainy winters; permits vegetation covers of maquis shrubland, Turkish pine (Pinus brutia), and oak forests (Quercus spp.), which support fire-prone and regenerating vegetation (Kavgacı et al., 2023; Atalay et al., 2014; Sabuncu and Özener2019). The dry season increases the risk of wildfires, as they are among the most critical factors that threaten biodiversity in this particular region by causing habitat loss and fragmentation.

According to Kavgacı et al., 2023 and Fernández-García et al., 2021, wildfires pose the greatest risk to biodiversity in these forests. The biodiversity in the forests of İzmir is quite striking; it shelters a wide variety of animals and host many endemic plant species. The forests play a very vital role in the balance of ecosystems and habitats for many species. Habitat loss and fragmentation, on the other hand, happen because these ecosystems are prone to forest fires. National forest service's records indicate that several of the largest forest fires in recent history have occurred in these regions, leading to the loss of vast forest areas, underscoring the need for effective monitoring and assessment strategies. From 2004 to 2022, İzmir was the third province in Türkiye with the highest number of forest fires: 4,622 incidents that burned an area of about 23,983 hectares. In 2022, the number of forest fire incidents was 293, with 1,300 hectares of burned areas (Kavgacı et al., 2023). Large fire events for this study took place in different years, like 2016, 2017, and 2019. These included both surface and crown fires. Forest management agents extinguished these fires after they had been burning for several days. We acquired historical records about the fire events from the official site of the General Directorate of Forestry.

Data Collection

Despite the availability of various satellite data sources, such as those from Landsat and MODIS, Sentinel-2 imagery was selected in this present study due to its optimal combination of spatial and temporal resolution and its rich spectral information. Among these sensors, Sentinel-2 has the finest spatial resolution (10 m) for the key visible and near-infrared bands, providing a more detailed delineation of burn scars compared with the resolution of 30-m offered by Landsat or the coarser resolution provided by MODIS (250-1000m) (Chuvieco et al., 2019). Because its revisit time is 5 days, Sentinel-2 has a higher chance of acquiring cloud-free imagery shortly after fire events compared to the 16-day cycle of Landsat.

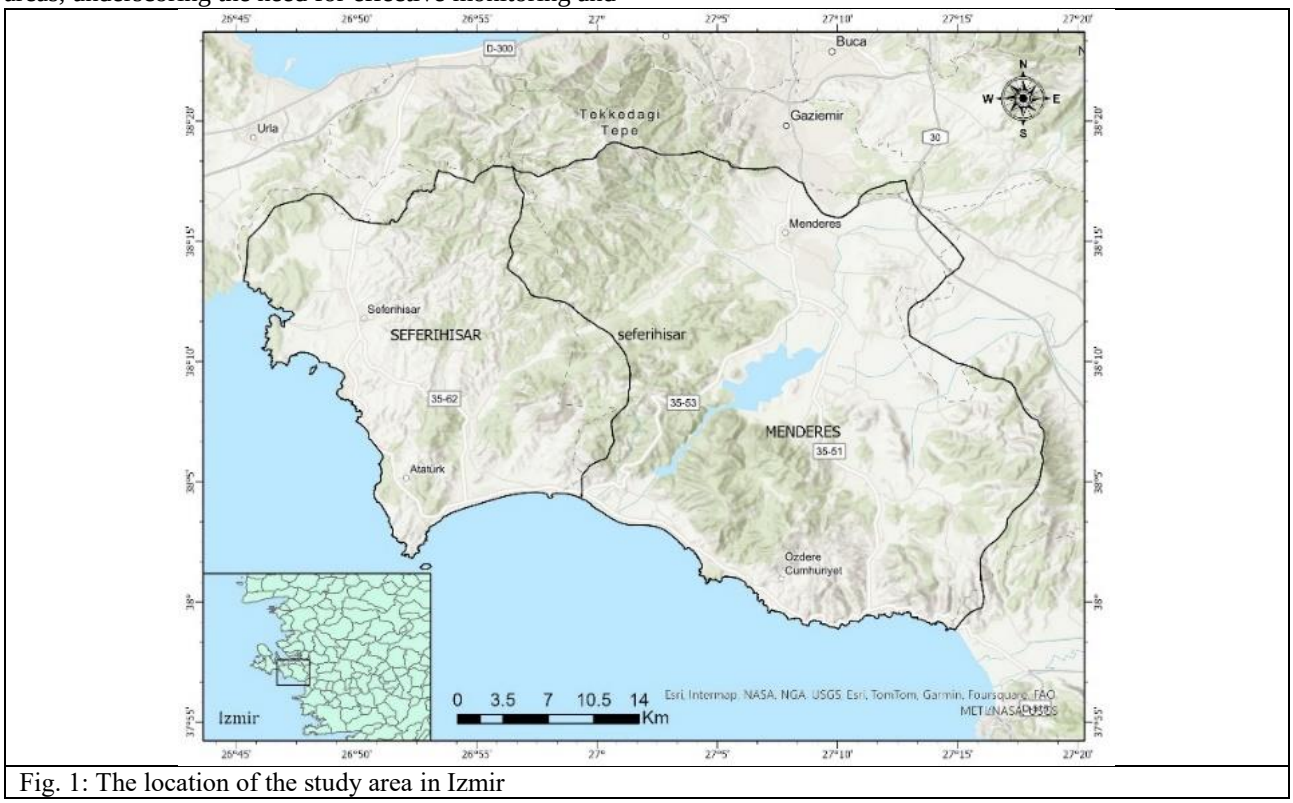

Fig. 1: The location of the study area in Izmir

Operated by the European Space Agency, Sentinel-2 provides a great opportunity to visualize and analyze the effects of wildfires. Significant fire events from 2016 to 2019 served as valuable case studies. Two key images were gathered from the Copernicus program for each fire incident, remarking on the situation before and after the fire. These images are instrumental in assessing the impact of the fire and understanding the land cover dynamics over time.

The Satellite System Sentinel-2 generates 13 spectral bands: 4 visible bands, 2 near-infrared bands, and 2 short-wave infrared bands, with 3 vegetation red edge bands and 2 for atmospheric correction. The spatial resolutions of

these bands range from 10 to 60 meters. The spectral bands and spatial resolutions make the Sentinel-2 mission of great value in giving detailed and accurate information about the earth's surface (Sentinel-2 Mission Overview, 2015).

Table 2.Sentinel-2 spectral bands and their characteristics

Bands	Central Wavelength (nm)	Resolution (m)
Band 1- Coastal Aerosol	443	60
Band 2 - Blue	490	10
Band 3 - Green	560	10
Band 4 - Red	665	10
Band 5 - Red Edge 1	705	20
Band 6 - Red Edge 2	740	20
Band 7 - Red Edge 3	783	20
Band 8 - Visible and Near Infrared (VNIR)	842	10
Band 8A - Narrow NIR	865	20
Band 9 - Water Vapor	945	60
Band 10 - SWIR - Cirrus	1375	60
Band 11 - SWIR 1	1610	20
Band 12 - SWIR 2	2190	20

In this respect, the data gathered from Sentinel-2 is key to capturing a holistic view of the post-fire landscape. In this regard, it provides detailed analysis and mapping of burned areas, changes in land cover, and the ecological impact of the wildfires in the study area. Supporting the analysis are also land cover maps and fire perimeter data from MODIS.

Such a data-driven approach gives invaluable insights into the future of wildfire management and ecological restoration. Understanding how fire-prone ecosystems function in a changing climate and with human impacts is critical to conserving the natural heritage of forest ecosystems. The study will aim to advance our understanding of the impacts of wildfires and develop better strategies for land management and ecological restoration.

Image processing and Classification

Prior to initiating image classification, it is imperative to undertake preprocessing procedures for the Sentinel-2 satellite data. Comprehensive pre-processing was performed to ensure that the data was accurate and reliable in the detection of areas of forest fires with Sentinel-2 imagery. First, the atmospheric correction of all Level-1C Sentinel-2 data is done using the Sen2Cor processor to convert them into Level-2A, which includes bottom-of-atmosphere reflectance values. The most important processing steps involved in creating the cloud and shadow masks included pixel masking with more than 50% cloud probability in the cloud probability layer. Detecting cloud shadows involved a modified version of the Google Earth Engine script by intersecting predicted shadow areas and low-reflectance near-infrared pixels. To facilitate multi-band analysis, all Sentinel-2 bands were harmonized to a common 10-meter spatial resolution. The shortwave infrared bands (B11 and B12), originally at 20-meter resolution, were resampled to 10 meters using the nearest neighbor interpolation method. This approach preserves the original pixel values while aligning the bands spatially (Mandanici and Bitelli, 2016). Subsets of the images were extracted using forest fire coordinates.

Image processing operations included histogram equalization and linear stretching to enhance the contrast between the burned and unburned forest areas. Reflectance in various bands was standardized through the process of min-max normalization, which rescales the reflectance values to a range of 0-255. To avoid crossing the memory limit of Google Earth Engine, this study mosaicked images obtained on close dates to produce a single image, thus reducing the number of images. In addition, co-registration and alignment with a map projection system were necessary to make it easier to look at Sentinel-2 satellite images and find changes Geometric correction serves to rectify distortions that stem from the representation of the Earth's curved surface in two dimensions within the imagery. This correction ensures that the data from different times aligns seamlessly, allowing for meaningful comparisons (Baillarin et al., 2012).

For land cover classification within the study area, a supervised classification approach was employed. This approach combined spectral information from the Sentinel-2 satellite images with a priori knowledge of the terrain. The Sentinel-2 sensor, with its high-resolution multispectral capability, was the source of data for the analysis. All bands available were used in a color composite from the Sentinel-2 images. The band combination used was 8-4-3, representing the Near Infrared, Red, and Green bands, respectively. This combination is selected because it has the capability of giving optimum visual contrast between various land cover categories (Delegido et al., 2011). To aid the classification, training areas were selected for all the land cover categories using the Area of Interest tools. Carefully computed were spectral signatures of those training areas. The classification categories used were the seven discrete classes generated from the early image and the later images. The classification was performed using the Maximum Likelihood classifier (MLC), which is a widely accepted parametric algorithm used for classifying remotely sensed imagery in the presence of probabilistic models, thus an important requirement for many monitoring environmental changes and land cover mapping exercises.

The Maximum Likelihood method uses the concept of multivariate normal distribution to assign pixels to pre-defined classes according to their spectral signatures (Foody, 2002; Richards, 2013). The Maximum likelihood classification is performed according to the following equation;

$$g_i(x) = ln\, P(w_i) - \frac{1}{2} ln|\Sigma_i| - \frac{1}{2}(x-\mu_i)^T \Sigma_i^{-1}(x-\mu_i), \quad \text{(Eq.1)}$$

where $g_i(x)$ is the discriminant function for class w_i, $P(w_i)$ is the prior probability of the class w_i, Σ_i is the covariance matrix of the class w_i, μ_i is the mean vector of the class w_i, x is the pixel vector, and $|\Sigma_i|$ is the determinant of Σ_i (Richards and Jia, 2006). This equation describes the probability distribution for a given set of data, facilitating classification by choosing the class with the highest probability.

A contingency error matrix and the Kappa coefficient were used to analyze the accuracy of the classification. An error matrix is a category-by-category comparison of the known reference data with the result of the automated classification. Error matrices provide information on accuracy measures such as overall accuracy, the user's accuracy, and the producer's accuracy. Overall accuracy is a basic measure that is calculated by dividing the total number of correctly classified pixels by the total number of reference pixels.

Simultaneously, the user's accuracy informs them of whether or not a given class on the map corresponds to the same class on the ground in the real world. The user's accuracy is calculated as follows:

$$User'sAccuracy = \frac{C_{ii}}{C_{i*}} \times 100\%, \qquad \text{(Eq.2)}$$

Where C_{ii} is the element at the position of the i-th row and i-th column, and C_{i*} is the row sum for class$i$.
On the other hand, the producer's accuracy serves to inform how well each class has been correctly classified (Congalton and Green, 2008). Producer's accuracy is calculated as:

$$Producer'sAccuracy = \frac{C_{aa}}{C_{sa}} \times 100\%, \qquad \text{(Eq.3)}$$

Where C_{aa} is the element at the position of the a -th row and the a -th column, and C_{sa} is the column sum for class a.

The weakness of these two measures is that they are limited in scope in the sense that they only inform about the performance of the classification strategy concerning the training areas (Congalton, 2015; Lillesand and Kiefer, 1994). To improve the interpretation of the error matrix, the Kappa coefficient was introduced. This coefficient helps in finding out whether or not the result that is represented on the error matrix is better than a random chance would provide (Congalton and Green, 2008; Foody, 2010). The Kappa coefficient is calculated as,

$$\kappa = \frac{N \sum_{i=1}^{r} x_{ii} - \sum_{i=1}^{r} (x_{i+} \cdot x_{+i})}{N^2 - \sum_{i=1}^{r} (x_{i+} \cdot x_{+i})} \qquad \text{(Eq. 4)}$$

Where r is the number of rows in the error matrix, x_{ii} is the number of the observations in row I and column i (the diagonal cells), x_{i+} is the total observations of row I, x_{+i} is the total observations of column i, and N is the total number of observations in the matrix. A kappa value of 1 indicates perfect agreement, while a value of 0 indicates no agreement better than chance (Foody, 2002).

These assessment methods of accuracy are very useful in verifying the performance of likelihood classification in remote sensing. For they, can be used quantitatively with the producer and user's accuracy, along with the kappa coefficient, to compare the performance of classification algorithms concerning the analysis of different remote sensing scenes, in which the classification results will be used for mapping land cover or monitoring the environment.

Principal component Analysis (PCA)

Principal component analysis is one of the central methods in multivariate statistics that provides a way of reorienting complex data sets along new axes, which capture maximum variance in data manner (Hotelling, 1933; Huang et al., 2022; Lanorte et al., 2015; Singh and Harrison, 1985). The procedure, although very old; with roots well into the beginning of the 20th century; has grown to become one of the most recognizable and widely used multivariate analysis tools. This is reflected in the broad spectrum of applications that PCA finds use in. It enables researchers to visualize complicated patterns of correlated datasets, removing redundancies, spotting anomalies, and compressing information. Of course, one of these strong points is the enhancement of the interpretability of data by reducing their dimensionality while retaining their essential characteristics. Such is the strength of PCA across a wide array of fields, from ecological ordination to machine learning applications for cluster analysis, feature selection, and enhancing statistical discrimination. Nevertheless, one should be aware of the limitations of PCA.

Although good for discovering the general structure of the data, it does not have any optimization criteria for class separation. Indeed, the transformation is based on global variance measures and includes dimensions which are not necessarily the most informative for a given classification task. This leaves the responsibility in most cases to the researcher to identify which principal components offer a high signal-to-noise ratio and relevant insights for some particular research question or application.

A Sentinel-2 image can be mathematically described in matrix format as follows:

$$X_{n,b} = \begin{pmatrix} x_{1,1} & \cdots & x_{1,n} \\ \vdots & \ddots & \vdots \\ x_{13,1} & \cdots & x_{13,n} \end{pmatrix} \qquad \text{(Eq.5)}$$

Where n is the number of pixels and b the number of bands. Considering each spectral band as vector, the aforementioned matrix can be simplified as follows:

$$X_k = \begin{pmatrix} x_1 \\ x_2 \\ \vdots \\ x_{13} \end{pmatrix} \qquad \text{(Eq.6)}$$

Where k is is the total number of bands. To achieve dimensionality reduction from the original bands, the eigenvalues of the covariance matrix have to be calculated. The description of this matrix is given as follows:

$$C_{b,b} = \begin{pmatrix} \sigma_{1,1} & \cdots & \sigma_{1,n} \\ \vdots & \ddots & \vdots \\ \sigma_{13,1} & \cdots & \sigma_{13,n} \end{pmatrix} \quad \text{(Eq.7)}$$

Where $\sigma_{i,j}$, is the covariance of each pair of different bands;

$$\sigma_{i,j} = \frac{1}{N-1}\sum_{p=1}^{N}\left(DN_{p,i} - \mu_i\right)\left(DN_{p,j} - \mu_j\right) \quad \text{(Eq.8)}$$

Where $DN_{p,i}$ is a digital number of a pixel p in the band $i, DN_{p,j}$ is a digital number of a pixel p in the band j, μ_i and μ_j are the average of the DN for the bands i and j, respectively.

The eigenvalues (λ) are obtained by solving the characteristic equation of the covariance matrix,

$$\det(C - \lambda I) = 0 \quad \text{(Eq.9)}$$

Where I represents the identity matrix with diagonal elements, and C symbolizes the covariance matrix of the bands.

The eigenvalues represent the amount of information contained in every band. By computing a ratio of individual eigenvalues with respect to their sum, the percentage of original variance captured by each principal component can be determined. This can be used to identify and remove components with the lowest variance, which contribute minimal information.

The principal components can be expressed in a matrix form as follows:

$$Y_{13} = \begin{pmatrix} y_1 \\ y_2 \\ \vdots \\ y_{13} \end{pmatrix} = \begin{pmatrix} w_{1,1} & \cdots & w_{1,13} \\ \vdots & \ddots & \vdots \\ w_{13,1} & \cdots & w_{13,13} \end{pmatrix} \begin{pmatrix} x_1 \\ x_2 \\ \vdots \\ x_{13} \end{pmatrix} \quad \text{(Eq.10)}$$

Where Y stands for the vector of the principal components, W is the transformation matrix, and X represents the vector of the original data. The transformation matrix (W) coefficients are eigenvectors that diagonalize the original bands' covariance matrix. These coefficients allow us to connect principal components with real variables, providing insights into their relationships. The eigenvectors can be calculated from the vector-matrix equation for each eigenvalue λ_k,

$$(\mathrm{C} - \lambda_k I)w_k = 0 \quad \text{(Eq.11)}$$

Where C is the covariance matrix, λ_k is the k eigenvalues, I is the diagonal identity matrix, and w_k is the k's eigenvectors.

The multi-temporal PCA analysis was conducted on satellite images from Seferihisar and Menderes in Izmir province. Images taken with Sentinel-2 in 2016 and 2019 were used in this study. The choice of principal components was made to cause the least possible loss of information while emphasizing the presence of vegetation and areas damaged by fire (Chuvieco et al., 2002). The choice of the bands was on bands B3, B4, B5, B8, B11 and B12. More specifically, components that contained detailed information about the burned areas were carefully inspected.

Normalized Difference Vegetation Index

The Normalized Difference Vegetation Index (NDVI) is one of the most commonly applied indices in remote sensing. It quantifies vegetation by measuring the difference between near infrared (NIR) and red (R) light reflected by vegetation. NDVI is an indicator of photosynthetic activity and general plant health; therefore, it is significantly useful in assessing vegetation cover and how it varies over time (Rouse et al., 1974). NDVI values vary between -1 and +1. The higher the value, the denser and healthier the vegetation; lower values indicate sparse or unhealthy vegetation. NDVI is more reliable while monitoring agricultural fields, forests, and natural vegetation cover (Tucker, 1979).

In the current study, NDVI values have been derived for the pre- and post-fire periods (2016 and 2019). The formula to compute NDVI is as follows:

$$NDVI = \frac{(NIR-RED)}{(NIR+RED)} \quad \text{(Eq.12)}$$

NIR represents the reflectance in the near-infrared band and Red is the reflectance in the red band; band 8 and band 4 from sentinel-2. NDVI values helped to differentiate between burned and unburned areas by analyzing the difference in vegetation indices between pre- and post-fire images. Fire-prone ecosystems typically experience significant impacts on vegetation cover, leading to a significant difference in NDVI values. By subtracting the NDVI values of the post-fire image from the pre-fire image, we can create an NDVI difference image:

$$\Delta NDVI = NDVI_{2019} - NDVI_{2016} \quad \text{(Eq.13)}$$

This image is useful for representing a forested area of severe change because large negative values correspond to a reduction in vegetation cover due to fire damage (Lutes et al., 2006).

The NDVI Thresholding Process

We used a combination of statistical analysis and expert knowledge to decide on threshold levels in the NDVI process. The mean and standard deviation of the NDVI difference values for the entire study area were calculated. We then defined a preliminary threshold as two standard deviations below the mean-a threshold that is generally considered to capture significant vegetation loss due to fire (Key and Benson, 2006).

The result was visually interpreted and the threshold further refined by comparing the classification output to high-resolution post-fire imagery and any available ground truth data. The threshold was selected at the point that maximized agreement between our classification and known burned areas, while minimizing commission errors (false positives) in unburned areas (Lillesand and Kiefer, 1994). The threshold selection has been validated by randomly choosing 100 points within the study area and

compared our classification result against a visual interpretation of high-resolution imagery. This resulted in an overall accuracy of 92%, with a Kappa coefficient of 0.84, showing strong agreement between our classification and reference data

The methodology used for the current study couples PCA with NDVI values to evaluate and map burned areas in the forests of western Türkiye. PCA is a data transformation method that allows for the possibility of a clear visualization of the areas characterized by multi-temporal dynamics. Thus, persistent land cover types correlate with the major features of the multi-temporal images, and the PCA components include areas characterized by significant dynamics. Each successive PCA component explains a smaller proportion of the total variance of the multi-temporal dataset. In this way, the integration of NDVI makes it possible to notice the dynamics in smaller areas (Lanorte et al., 2015; Lasaponara, 2006). Fig. 2 illustrates the complete approach followed to achieve the purpose of this study:

Results and Discussion

Remote sensors face many choices and challenges when using multi-temporal satellite data to map burned areas of mixed forest ecosystems. Our study hereby demonstrates these aspects with greater precision in relation to MLC for burned areas mapping across three clearly distinct fire events in 2016, 2017, and 2019. Though the general accuracy of MLC was very high, the accuracy of the burned area category was different among these three fire events. This is a common variability in remote-sensing studies of complex landscapes, mainly when dealing with fires of different scales and intensities in such studies (Petropoulos et al., 2011; Gigović et al., 2019).

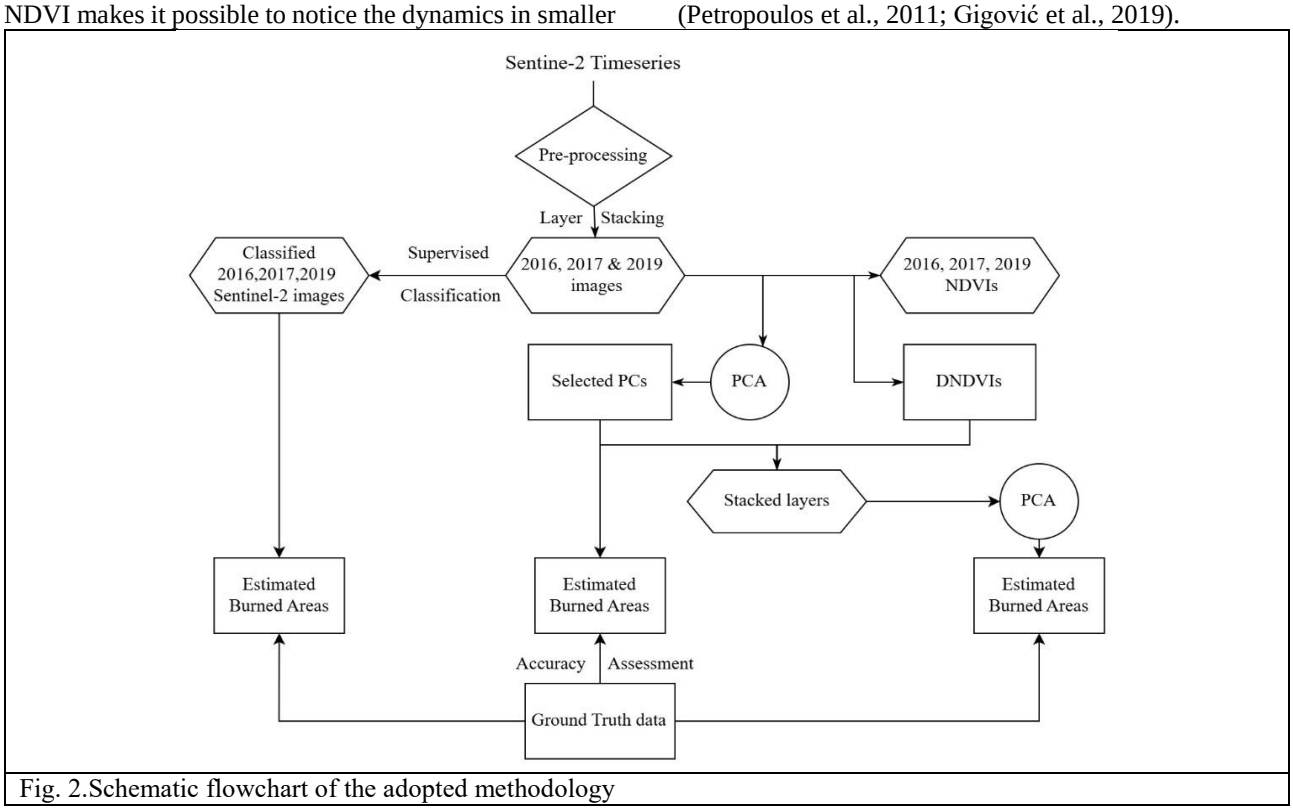

Fig. 2.Schematic flowchart of the adopted methodology

Several factors complicate the supervised classification of burned areas, particularly when dealing with multiple fire events over years. The spectral signatures for burned areas are still highly variable due to burn severity, pre-fire vegetation types, and time passed since the burning occurred (Lentile, et al., 2006). Moreover, this further complicates the problem of fires, as they can burn at varying magnitudes and in different years, each with its own unique characteristics. Furthermore, a high spectral overlap of burned areas with dark surfaces, such as water bodies and shadows on steep terrain, along with certain types of bare soil or rock, typically results in classification errors (Bastarrika et al., 2011; Mallinis and Koutsias, 2012). For the 2016 and 2017 fire events, our supervised classification gave overall accuracies of 96.80% and 96.53%, respectively in comparison with ground truth area. The ground-truth data was retrieved from field survey reports and an official map provided by the General Directorate of Forestry. This result provides insight into our classification method's overall strengths under varying fire incidences. The slight increment in 2019 with an overall accuracy of 97.86% is probably because of the large scale of the 2019 fire incident which made its distinction much easier (Liu et al., 2020). Focusing on the class's burned area for each fire event reveals some interesting patterns. The user's accuracy for burned areas was high in all years, which indicates that the identification of those specific burned areas was perfect, presenting a low amount of false positives. For the 2019 fire event, the accuracy decreased slightly to 95.08% compared to the fire incidents in 2016, and 2017, which may be due to the larger and possibly more complex nature of such fires.

Table 3: Error Matrix of Classified Sentinel-2 Acquired in 2016

	Water	Forest	Planted/ Cultivated	Developed	Rangeland	Barren	Burned area	Total	User's accuracy (%)
Water	35	0	0	0	0	0	0	35	100
Forest	2	260	1	0	7	0	0	270	96.30
Planted/ Cultivated	0	0	133	4	0	0	0	137	97.08
Developed	0	0	1	88	0	0	0	89	98.88
Rangeland	0	6	0	0	156	0	2	164	95.12
Barren	0	0	0	0	1	20	0	21	95.24
Burned area	0	0	0	0	0	0	34	34	100
Total	37	266	135	92	164	20	36	750	
Producer's accuracy (%)	94.59	97.74	98.52	95.65	95.12	100	94.44		96.80

Table 4: Error Matrix of Classified Sentinel-2 Acquired in 2017

	Water	Forest	Planted/ Cultivated	Developed	Rangeland	Barren	Burned area	Total	User's accuracy (%)
Water	35	0	0	0	0	0	0	35	100
Forest	2	252	1	0	7	0	0	262	96.18
Planted/ Cultivated	0	0	128	5	0	0	0	133	96.24
Developed	0	0	2	90	0	0	0	92	97.83
Rangeland	0	6	0	0	164	0	2	172	95.35
Barren	0	0	0	0	1	20	0	21	95.24
Burned area	0	0	0	0	0	0	35	35	100
Total	37	258	131	95	172	20	37	750	
Producer's accuracy (%)	94.59	97.67	97.71	94.74	95.35	100	94.59	0.00	96.53

Table 5: Error Matrix of Classified Sentinel-2 Image Acquired in 2019

	Water	Forest	Planted/ Cultivated	Developed	Rangeland	Barren	Burned area	Total	User's accuracy (%)
Water	39	0	0	0	0	0	0	39	100
Forest	0	253	3	0	0	0	1	257	98.44
Planted/ Cultivated	0	1	133	1	0	0	0	135	98.51
Developed	0	0	0	105	0	0	0	105	100.00
Rangeland	1	3	0	0	130	0	0	134	97.01
Barren	0	0	0	0	3	16	0	19	84.21
Burned area	0	1	0	0	2	0	58	61	95.08
Total	40	258	136	106	135	16	59	750	
Producer's accuracy (%)	97.50	98.06	97.79	99.06	96.30	100	98.30	0.00	97.86

Table 6: Total Accuracy and Kappa Coefficient of Maximum Likelihood Classified Sentinel-2 Images

	2016 Classification		2017 Classification		2019 Classification	
	User's accuracy (%)	**Producer's accuracy (%)**	**User's accuracy (%)**	**Producer's accuracy (%)**	**User's accuracy (%)**	**Producer's accuracy (%)**
Water	100.00%	94.59%	100.00%	94.59%	100.00%	97.50%
Forest	96.30%	97.74%	96.18%	97.67%	98.44%	98.06%
Planted/ Cultivated	97.08%	98.52%	96.24%	97.71%	98.52%	97.79%
Developed	98.88%	95.65%	97.83%	94.74%	100.00%	99.06%
Rangeland	95.12%	95.12%	95.35%	95.35%	97.01%	96.30%
Barren	95.24%	100.00%	95.24%	100.00%	84.21%	100.00%
Burned Area	100.00%	94.44%	100.00%	94.59%	95.08%	98.30%
Overall Accuracy (%)	96.80%		96.53%		97.86%	
Kappa Coefficient	0.95		0.95		0.97	

The progressive improvement in the accuracy of the producer perception during all three-fire events, successively, was 94.44% in 2016, 94.59% in 2017, and 98.30% in 2019. This trend would prove an amelioration of our perception of detecting the whole extent of burned areas over time and acknowledge different gradients of fire intensity (Roteta et al., 2019).

The variation in accuracy across the three fire events highlights challenges in developing a single classification approach that would perform equally effectively for fires of different sizes and intensities. One plausible reason for the discrepancy between the user's accuracy of the 2019 fire and the producer's increased accuracy is our method's superior sensitivity in detecting a larger burned area, albeit at a slight additional cost in false positives. This sensitivity-specificity trade-off can be more pronounced with different sizes and magnitudes of fires (Chuvieco et al., 2019). Fire characteristics such as intensity, severity, and extent can have a significant impact on the spectral signature of burned areas and, consequently, the accuracy of their identification. A highly intense fire such as the 2019's fire incident, that consumes the majority of the vegetation typically results in a very important spectral signature and thus provides higher classification accuracy. Because of this, it will be hard to make accurate classifications when low-intensity fires or fires that happen in areas with few plants cause subtle changes in the reflectance signature (Lentile, et al., 2006). Moreover, the elapsed time between the fire event date and image acquisition may influence the mapping accuracy.

Fresh burn scars usually have more striking spectral signatures; in older scars, however, vegetation regrowth might have already distinctly changed their spectral features (Chu and Guo, 2013). Most of the time, we observe slight variations in classification accuracies for our burns across different years, indicating that each fire event must have had unique characteristics in terms of intensity, extent, and the time between the fire and image acquisition. Despite these high accuracies, the separation of burned areas from other classes of land cover that are spectrally similar has been challenging. In general, this forms a common challenge in burned area mapping, while in heterogeneous landscapes, burned areas may spectrally be very similar to other darksurfaces like water bodies, shadows, or specific types of soil classes. The results of these analyses and their implications for burned area mapping are presented hereinafter. PCA was applied to a stacked raster of six bands selected from the 2019 Sentinel-2 image. The choice of these bands is based on their sensitivity to fire-induced changes and their ability to capture different landscape characteristics.

Table 7 indicates how the different bands have contributed to the principal components. Strong negative loadings are noticed in all bands, with PC1, and especially band 5 with values of -0.53, would point towards this representing the overall brightness or albedo. A very strong positive loading for PC2 lies on band 4, with a value of 0.89 compared to the negative loadings on the other bands. This is likely the contrast between visible and NIR/SWIR bands and may turn out to be informative in vegetation analyses.

Model performance was evaluated using the percentage of correctly classified observations. The most efficient models were used to map burned areas for the entire dataset. The second PCA was performed on stacked bands 4, 8, 1, and 12 from both 2016 and 2019 imagery (Table 8). These bands were selected based on their capability in discriminating the burned areas efficiently. This has been done in order to look at a more specific part of the spectral bands to enhance the burned area detection. In this analysis, PC1 accounts for 75.65% of the variance, slightly less than in the 2019-only analysis. The first four components cumulatively explain 97.14% of the total variance, indicating that most of the information, including temporal changes, is captured in these components. The interesting patterns observed in PC4 and PC5 are likely to be more relevant to the detection of burn scars, as they reflect the evolution between 2016 and 2019. The strong contrasts among corresponding bands of different years (e.g., Band 4 of 2016 vs. Band 4 of 2019) represented by the loadings within these components might be indicative of an area that experienced strong change, most probably by fire.

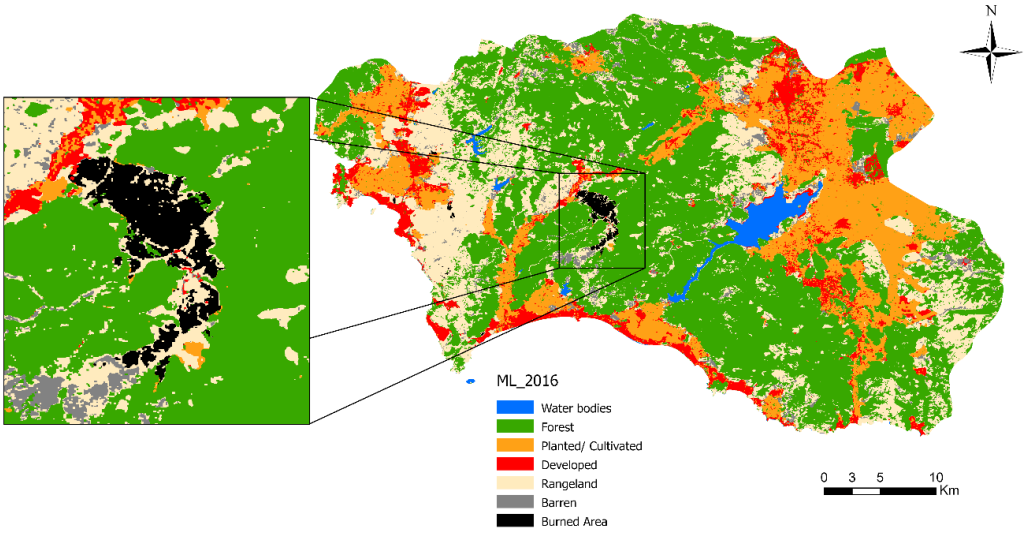

Fig. 3: Maximum Likelihood Classified Sentinel-2 Image from 2016

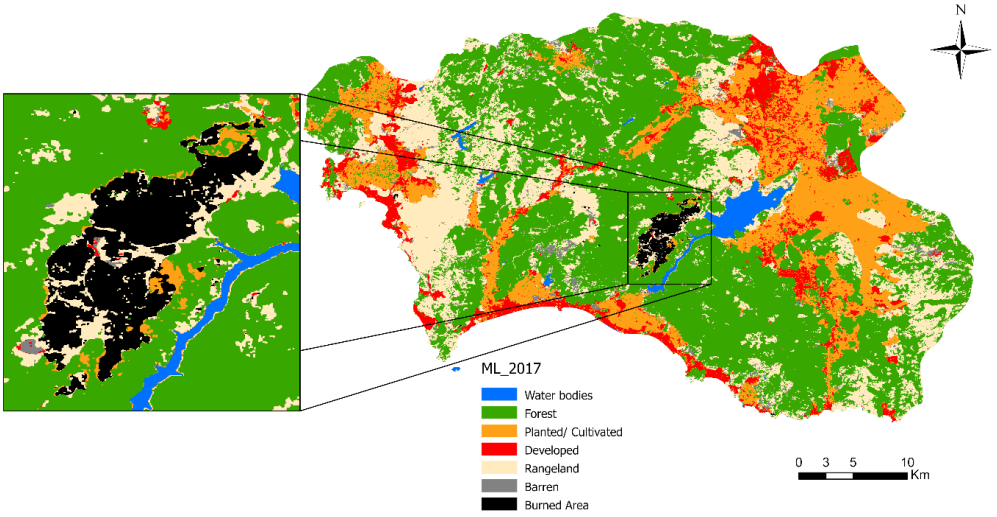

Fig. 4: Maximum Likelihood Classified Sentine-2 from 2017.

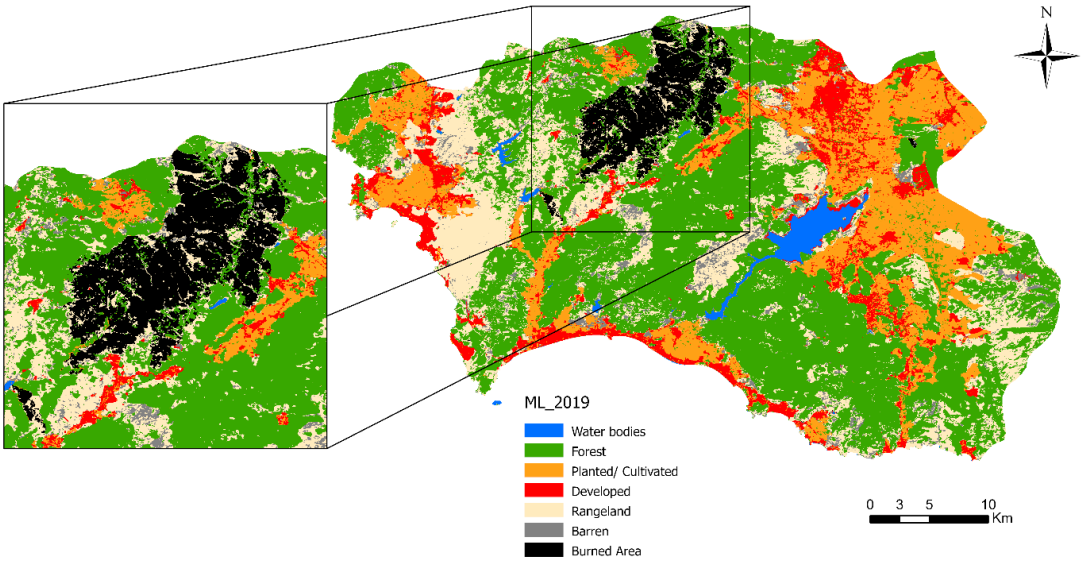

Fig. 5: Maximum Likelihood Classified Sentinel-2 from 2019.

Table 7: PCA of the 2019 Sentinel-2 Image. Note the strong negative loadings in PC1 across all bands, indicating overall brightness, and the strong positive loading for Band 4 in PC2, suggesting its importance in vegetation analysis

	PC1	**PC2**	**PC3**	**PC4**	**PC5**	**PC6**	**PC7**	**PC8**
Eigenvalue	0.09	0.02	0.01	0.00	0.00	0.00	0.00	0.00
% Eigenvalue	75.65	13.28	5.50	2.71	2.23	0.31	0.24	0.08
Cumulative %	75.6	88.9	94.4	97.1	99.4	99.7	99.9	100.0
Bands	**Eigenvectors**							
B3-16	-0.36	-0.19	-0.36	-0.40	-0.46	-0.48	0.30	0.12
B4-16	-0.29	0.46	-0.40	0.67	-0.28	0.04	0.01	-0.13
B8-16	-0.40	-0.13	-0.41	-0.09	0.43	0.50	0.11	0.45
B11-16	-0.31	-0.16	-0.27	-0.21	0.21	-0.05	-0.57	-0.62
B3-19	-0.35	-0.24	0.40	-0.03	-0.58	0.56	-0.10	-0.07
B4-19	-0.35	0.75	0.33	-0.40	0.10	-0.07	-0.11	0.11
B8-19	-0.43	-0.17	0.36	0.22	0.36	-0.16	0.56	-0.36
B11-19	-0.31	-0.26	0.27	0.36	0.07	-0.42	-0.48	0.48

Table 8: Multi-temporal PCA of Sentinel-2 images from 2016 and 2019. Observe how the first four components explain 97.14% of the total variance, capturing most of the temporal changes between the two years

	PC1	**PC2**	**PC3**	**PC4**	**PC5**	**PC6**
Eigenvalue	0.06	0.01	0.00	0.00	0.00	0.00
%Eigenvalue	78.5	16.8	3.93	0.41	0.27	0.09
Cumulative%	78.5	95.3	99.24	99.6	99.9	100
Bands	**Eigenvectors**					
B2	-0.28	-0.18	-0.42	-0.32	-0.47	-0.62
B3	-0.32	-0.12	-0.46	-0.19	-0.23	0.76
B4	-0.45	-0.25	-0.36	0.56	0.51	-0.16
B8	-0.43	0.89	-0.04	-0.08	0.10	-0.06
B11	-0.53	-0.14	0.59	0.35	-0.47	0.05
B12	-0.38	-0.28	0.35	-0.65	0.48	-0.01

Later, vegetation indices were included in more detail to explain their contribution to PCA using NDVI data for both 2016 and 2019 (Table 9). The uneven spread of variance across components observed in the previous analyses (Table 8) was likely driven by variance in the input spectral traits; the addition of NDVI data seems to ameliorate this issue by spreading the explained variance more evenly across the principal components

This decrease in the variance of NDVI distribution across components strongly suggests that the integration of NDVI has added non-redundant information compared to the earlier analysis. The information collected from the NDVI data is clearly distinct and independent; but complementary to the information collected from the spectral band data. The detailed patterns of landscape dynamics, especially those of change in burn scars, is much better captured by data from both spectral and vegetation index data.

The fluctuation of PC3 and PC4 exhibits a distinct pattern that is particularly relevant for burn scar recognition, while explaining a smaller percentage of the overall variance. The loading correspondence or opposition of spectral bands against NDVI value might occur more starkly for vegetation health change, which perhaps in most of the manifestations could be the result of fire damage.

As such, in the final analysis, we substituted NDVIs in the single bands with $\Delta NDVI$ representing the NDVI difference between 2019 and 2016. We note in the table below that PC1 represents 69.20% of the variance, while PC2 represents 15.14% of it. These together represent an additional 12.81% variance. Fig. 13 shows that the addition of $\Delta NDVI$ seems to increase the separation of the burned areas.

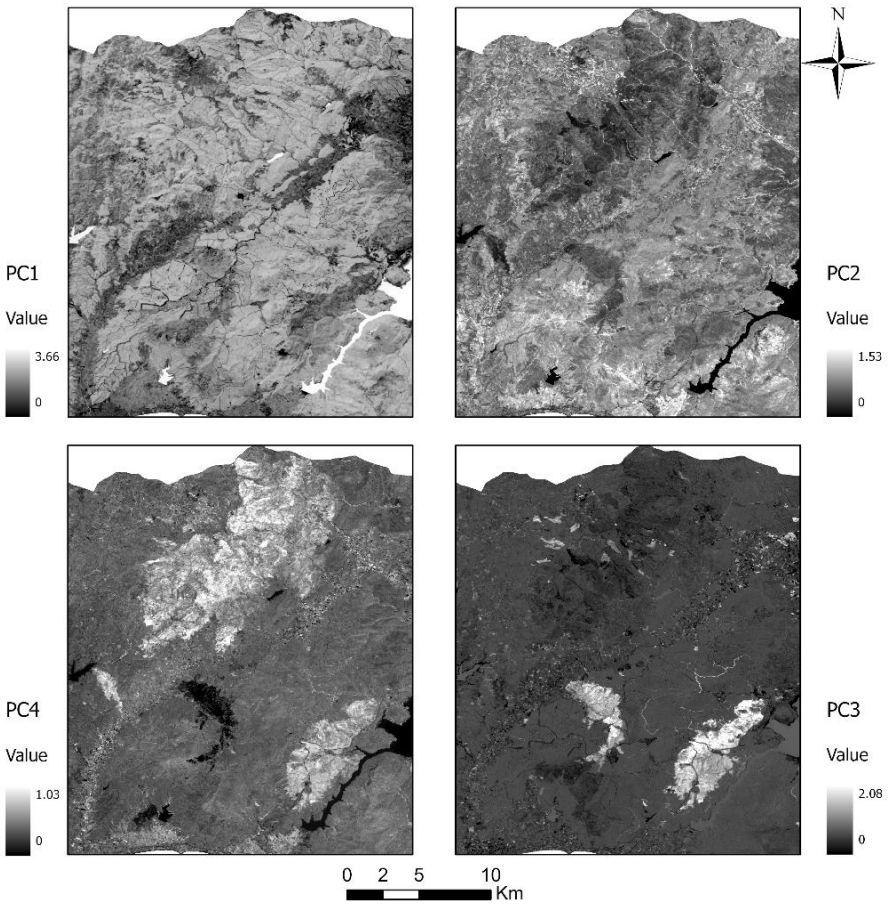

Fig. 6: PCA results showing (a) PC1, representing overall landscape brightness, (b) PC2, highlighting vegetation contrasts, (c) PC3 and (d) PC4, emphasizing areas of significant change potentially related to burn scars.

Table 9: Multi-temporal PCA of Sentinel-2 images and NDVI for 2016 and 2019. Note how the inclusion of NDVI spreads the explained variance more evenly across components, indicating its contribution of non-redundant information.

	PC1	**PC2**	**PC3**	**PC4**	**PC5**	**PC6**	**PC7**	**PC8**	**PC9**	**PC10**
Eigenvalue	0.10	0.04	0.01	0.01	0.00	0.00	0.00	0.00	0.00	0.00
% Eigenvalue	61.2	25.0	5.88	4.15	2.38	0.63	0.31	0.19	0.10	0.06
Cumulative %	61.3	86.3	92.2	96.3	98.7	99.3	99.7	99.8	99.9	100
Bands	**Eigenvectors**									
B3-16	-0.36	-0.02	0.27	-0.26	-0.27	-0.53	-0.27	0.08	0.54	0.10
B4-16	-0.23	0.35	-0.25	-0.53	-0.43	0.25	-0.28	0.11	-0.37	-0.11
B8-16	-0.39	0.07	0.16	-0.38	0.39	0.12	0.51	0.22	-0.07	0.45
B11-16	-0.30	0.01	0.18	-0.22	0.23	-0.03	0.19	-0.59	-0.01	-0.63
NDVI-16	0.26	0.38	-0.66	-0.20	0.15	-0.31	0.26	-0.08	0.34	-0.02
B3-19	-0.35	-0.07	-0.20	0.34	-0.26	-0.55	0.33	0.08	-0.48	-0.04
B4-19	-0.28	0.55	0.11	0.47	-0.30	0.34	0.22	-0.16	0.31	0.09
B8-19	-0.41	0.04	-0.25	0.25	0.44	0.10	-0.29	0.50	0.15	-0.37
B11-19	-0.31	-0.06	-0.30	0.12	0.25	-0.01	-0.44	-0.54	-0.11	0.48
NDVI-19	0.21	0.64	0.40	0.07	0.32	-0.35	-0.24	0.04	-0.31	0.02

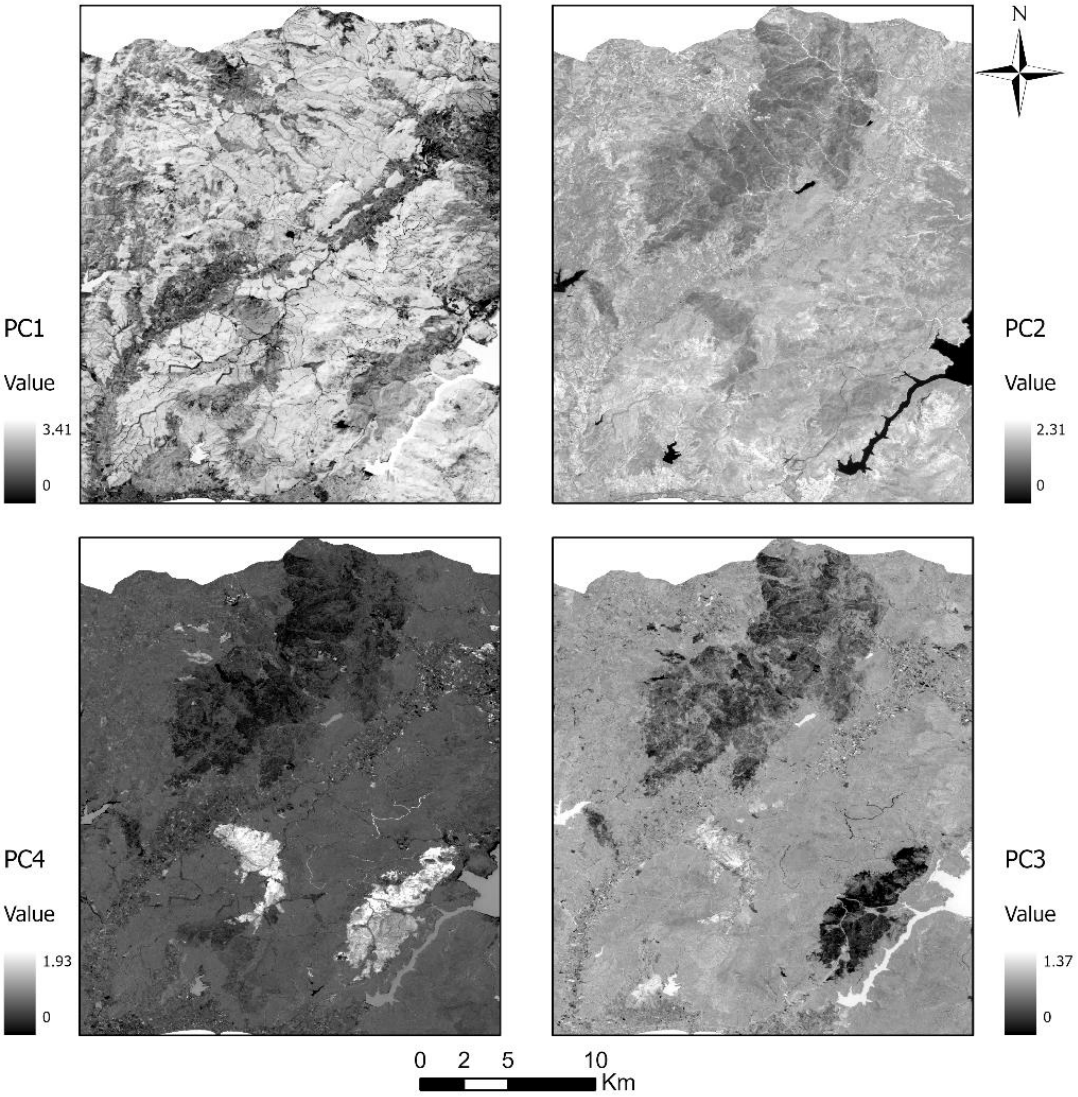

Fig. 4.PCA results incorporating NDVI data. (a) PC1, representing overall landscape structure and vegetation density; (b) PC2, highlighting contrasts between vegetation types and potential burn areas; (c) PC3, emphasizing vegetation changes that may indicate burn scars or recovery; (d) PC4, showing finer details of landscape variability potentially related to burn severity or recovery stages.

This is especially true in PC3 and PC4. The highest loading of $\Delta NDVI$, has 0.59 loading on PC2 and -0.61 loading on PC3; this would thus imply that the two components are vital in capturing dominant changes of vegetation over time that are relevant for the correct detection of burn scars. The results of PCA are shown in Fig. s 6, 7, and 8. In all these cases, visual analysis further supports and extends the insights obtained from the numerical data. On the other hand, standard PCA, as shown in Fig. 6, underlines the general landscape structure in PC1, while PC3 and PC4 specify high-contrast areas that might eventually indicate significant changes. Fig. 7, including NDVI, strengthens the discriminatory capability of vegetation patterns in both PC2 and PC3, thus highlighting probable burn scars more than regular PCA would. Most importantly, the PCA including $\Delta NDVI$, shown in Fig. 8, shows maximum contrast, mainly in PC2, with dark areas probably indicating huge losses in vegetation, characteristic of burn scars. PC3 and PC4 can give additional information on vegetation change in this analysis, which may indicate different stages of burn severity or recovery. This graphical evidence corresponds quite agreeably to the numerical findings, especially how, in Table 10, $\Delta NDVI$ has strong loadings in PC2 at 0.59 and PC3 at 0.62. The clear separation of the burned areas in PCA based on $\Delta NDVI$, especially visible in PC2 and PC3, further confirms the applicability of the method for semi-automated burn area mapping. These results show the effectiveness of multi-temporal PCA for burn-area detection and characterization, mainly when associated with vegetation indices. The technique can be a helpful tool for enhancing the accuracy and detail of burned area mapping in complex forest ecosystems, able to detect burns at different intensities and stages of recovery. Age classes of burn scars from individual fire events were mapped using the multi-temporal PCA applied to Sentinel 2 bands and the $\Delta NDVI$ index. The large 2019 fire is green is obvious, having a quite different spectral signature than the surrounding, older burn scars from 2017 and 2016. Another small burn scars appeared to have the same color, which means that they are recent.

Table 10: Statistics of Temporal NDVI Differencing. This table summarizes the NDVI values for 2016 and 2019, as well as their difference (ΔNDVI), providing insight into overall vegetation changes in the study area

	NDVI-2016	NDVI-2019	$\Delta NDVI$
Minimum values	-0.44	-0.41	-0.67
Maximum values	0.77	0.79	0.64
Mean values	0.35	0.34	0.01
Standard deviation	0.16	0.17	0.1

This is particularly evident in the PC2 and PC3 components of the $\Delta NDVI$-based PCA, where the 2019 burn scar represents a darker area facing the highest recent vegetation loss. In Fig. 9, the burn scars from 2017 and 2016 have varying contrasts, probably due to the different stages of vegetation recovery. This observation validates Veraverbeke et al. (2011)'s assertion that multi-temporal vegetation indices can effectively monitor post-fire vegetation recovery. The color variation between these older burn scars is very fine, suggesting that revegetation occurred gradually with the 2016 scar in a more advanced state of recovery than the 2017 scar. These findings align with the findings of Röder et al. (2008), who reported that Mediterranean ecosystems typically show rapid initial recovery, followed by a gradual regeneration process over time. These results, with a clear difference between recent and older burn scars, prove the sensitivity of the method for detecting acute fire damage and long-term recovery dynamics.

Upon evaluating the computed burned areas from the MLC and temporal PCA-based $\Delta NDVI$ against the observed burned areas for three fire events (2016, 2017, and 2019), the results in table 12 were found. These findings provide key insights into the effectiveness of these methods across different temporal scales.

According to the above table, the multi-temporal PCA based $\Delta NDVI$ performed the best for a recent fire in 2019, mapping about 98.76% of the officially reported area, while Maximum Likelihood Classification (MLC) overestimated this parameter at 111.29%, and there is a major overestimation by MODIS of about 136.00%. It is important to mention at this stage that the accuracy of the multi-temporal PCA method for mapping recent burn scars is higher, which conforms with the analysis by Veraverbeke et al. (2010) on the basics of multiple time periods used in fire impact assessment. Performance varied across fire years for all methods, which mirrors the complexities in mapping burn scars over time in Mediterranean-type ecosystems.

For the 2017 fire, all methods overestimated the burned area: MODIS by 178.40%, PCA by 128.50% and MLC by 106.36%. This may indicate overestimation because these methods account for secondary fire effects or further landscape-level changes beyond the initial burn scar, as noted by Díaz-Delgado et al. (2002). For the oldest fire event (2016), all methods returned overestimation, but with the highest overestimation expressed by PCA-based $\Delta NDVI$ at 125.34%, followed by the high-resolution MODIS data at 107.20%, with an overestimation of 103.38% by MLC. This systematic overestimation thus challenges the supposition of Röder et al. (2008) regarding the difficulty of mapping historical burn scars in rapidly recovering ecosystems. It would instead suggest that all methods could be sensitive to long-term landscape changes, which might easily be confused with burn scars.

Table 11: Multi-temporal PCA of Sentinel-2 images and ΔNDVI. Observe the high loadings of ΔNDVI in PC2 and PC3, highlighting its importance in capturing vegetation changes over time, crucial for burn scar detection.

	PC1	**PC2**	**PC3**	**PC4**	**PC5**	**PC6**	**PC7**	**PC8**	**PC9**
Eigenvalue	0.10	0.02	0.01	0.01	0.00	0.00	0.00	0.00	0.00
% Eigenvalue	69.20	15.14	8.03	4.78	2.07	0.37	0.23	0.12	0.07
Cumulative %	69.20	84.34	92.36	97.14	99.21	99.59	99.81	99.93	100
Bands	**Eigenvectors**								
B3-16	-0.36	-0.08	-0.32	-0.25	-0.57	-0.27	0.09	0.54	0.01
B4-16	-0.29	0.25	0.48	-0.61	-0.07	-0.29	0.09	-0.39	-0.04
B8-16	-0.40	-0.05	-0.25	-0.33	0.37	0.53	0.22	0.03	0.44
B11-16	-0.31	-0.07	-0.27	-0.17	0.13	0.20	-0.58	-0.11	-0.63
B3-19	-0.35	-0.26	0.04	0.36	-0.55	0.29	0.12	-0.52	0.04
B4-19	-0.36	0.62	0.38	0.35	-0.04	0.25	-0.19	0.35	0.03
B8-19	-0.43	-0.19	0.06	0.32	0.42	-0.31	0.50	0.08	-0.38
B11-19	-0.30	-0.29	0.07	0.19	0.19	-0.44	-0.54	-0.06	0.51
$\Delta NDVI$	-0.06	0.59	-0.62	0.16	0.03	-0.29	0.07	-0.37	0.09

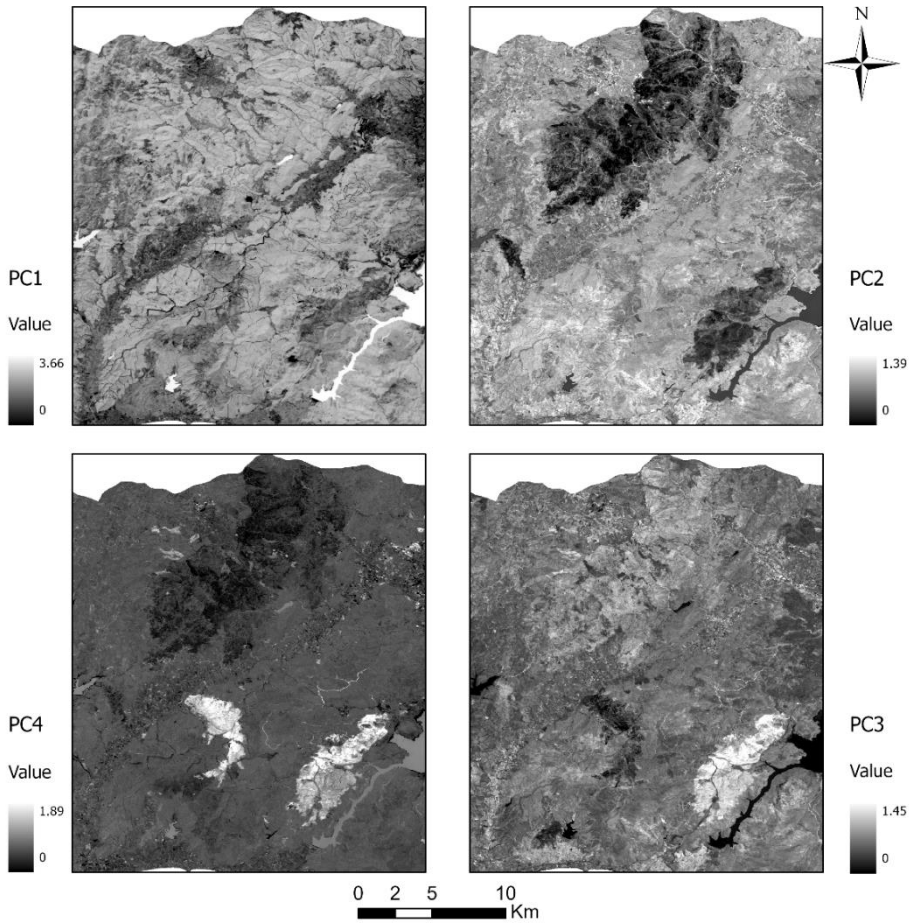

Fig. 5. PCA results incorporating ΔNDVI (NDVI difference between 2019 and 2016). (a) PC1, representing stable landscape features; (b) PC2, strongly highlighting areas of significant vegetation change, with dark areas likely indicating severe burns; (c) PC3, further differentiating burn scars and showing potential recovery patterns; (d) PC4, capturing subtler changes that may relate to burn severity gradients or different stages of vegetation recovery.

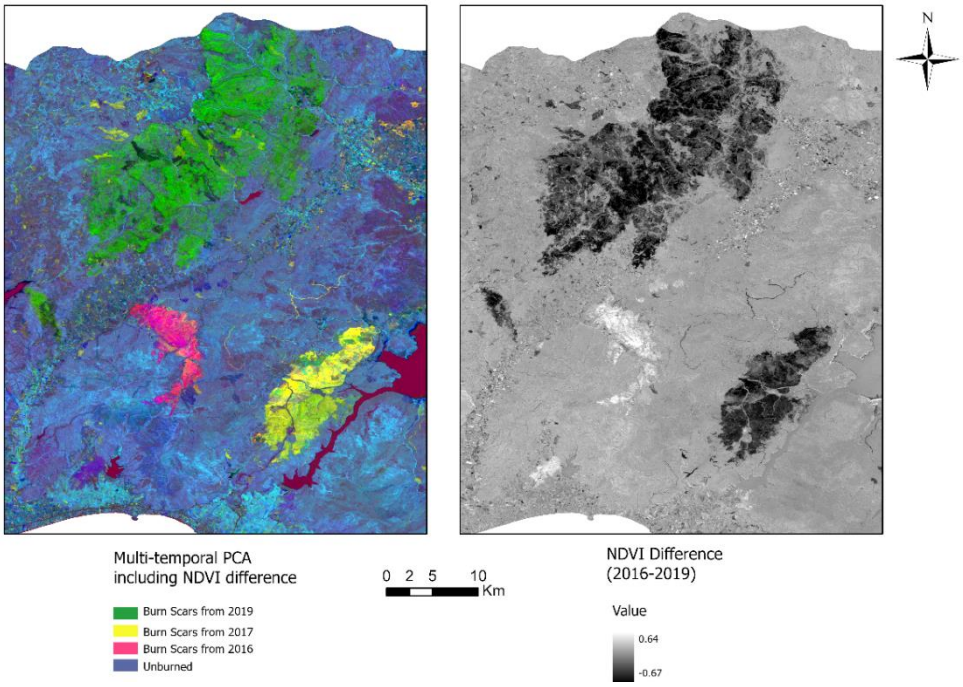

Fig. 6. Multi-temporal PCA results showing age classes of burn scars. Recent burn scars (2019) appear in green, exhibiting a distinct spectral signature compared to older burn scars from 2017 and 2016. Color variations between older scars indicate different stages of vegetation recovery, with 2016 scars showing more advanced regeneration than 2017 scars.

Table 10: Comparison of observed, MODIS and computed Burned Areas (BA) for the three fire incidents. Note the increasing overestimation trend for older fire events across all methods.

Fire Year	Officially Reported BA (ha)	MODIS BA (ha)	MLC BA (ha)	PCA-Δ$NDVI$ BA (ha)
2019	5000	6800.00 (136.00%)	5564.45 (111.29%)	4938 (98.76%)
2017	986	1759.00 (178.40%)	1048.74 (106.26%)	1267 (128.50%)
2016	500	536.00 (107.20%)	516.88 (103.38%)	626.69 (125.34%)

Table 11: Analysis of Accuracy Metrics for 2019 Fire Incident. This table provides a detailed breakdown of the accuracy assessment, comparing the PCA-based method with the MLC method for the most recent fire event

Metric	Fire Incident 2019
Total Study Area (ha)	116844.34
MLC Burned Area (ha)	5564.45
PCA Classified Burned Area (ha)	4938.71
True Positive (TP) Area (ha)	4730.20
False Positive (FP) Area (ha)	833.92
False Negative (FN) Area (ha)	208.51
Overall Accuracy (%)	81.94
User's Accuracy (%)	85.01
Producer's Accuracy (%)	95.78
Omission Error (%)	0.04
Commission Error (%)	0.15

The overestimation of burned areas in older fire events could be attributed to several factors. Firstly, vegetation regrowth in Mediterranean ecosystems is often rapid, which can confound spectral signatures over time. Secondly, other landscape changes unrelated to fire, such as drought stress or land use changes, may be misclassified as burn scars. To mitigate these issues in future studies, integrating higher temporal resolution data to capture the trajectory of vegetation recovery more precisely could be beneficial. Additionally, incorporating ancillary data such as topography, climate, and vegetation type could help distinguish fire-related changes from other landscape dynamics.

The accuracy assessment for the fire incident in 2019 conveys information on how well the PCA-based method performs as compared to what obtains using the MLC method. It should be noted that although an official estimation of the burned area has been given by the concerned authorities, the spatial perimeter data of this is not available, that puts a limitation on carrying out a comprehensive ground truth validation. For the total study area of 116,844.34 ha, the MLC method estimated a larger burned area of 5564.45 hectares compared to the PCA method's 4938.71 ha.

Compared to the reference data classified by MLC, the PCA method returned an overall agreement of 81.94%. The high producer's accuracy of 95.78% argues that a vast majority of areas classified as burned by the MLC are identified by the PCA method. This is further supported by a low omission error of 0.04, arguing that areas classified as burned by the MLC are rarely missed by PCA. The user accuracy of 85.01% and the commission error of 0.15 show that some areas are classified as burned by PCA that are not by MLC, which might point out to higher sensitivity in PCA or even possible over-classification.

This agreement between both methods is represented by a true positive area of 4730.20 ha, and these differences are underlined by false positives of 833.92 ha and false negatives of 208.51 ha. By these measures, it is shown that on one hand there is major consensus between PCA and MLC methods; on the other hand, there are certain significant differences. The discrepancies may be caused by the fact that the PCA method is more sensitive to slight burn signatures or due to overestimation by the MLC method.

While our study focused on comparing our PCA-NDVI method with MLC, it is worth noting that other machine learning approaches like Random Forest and Support Vector Machines have shown promise in burn scar mapping. These methods often excel in handling complex, non-linear relationships in spectral data. However, our PCA-NDVI approach offers the advantage of being more interpretable and computationally efficient, while still achieving high accuracy, especially for recent burn scars.
That is to say, while the multi-temporal PCA-based Δ$NDVI$ method may vary within the years of fire; from

slight underestimation in recent fires to huge overestimation in older fires; it works well for recent burn scar mapping but may need some refinement and integration of more time series data to track the regeneration state in historical burn scars. This variability thus underlines the complexity of mapping burn scars in fire-prone ecosystems. In this regard, it needs adaptive methods that can encompass the existing diversity of landscape dynamics occurring postfire.

Conclusion

This research demonstrates the effectiveness of integrating multi-temporal principal component analysis with vegetation indices to improve burned area detection and mapping within Izmir's forest ecosystems. The application of PCA to Sentinel-2 data, especially integrated with NDVI and $\Delta NDVI$, reveals a significant over-improvement on the accuracy front compared to conventional techniques, particularly in identifying recent burn scars.

The multi-temporal PCA method, incorporating $\Delta NDVI$ as a variable, showed highly promising results for mapping areas severely affected by forest fires. Notably, PC2 and PC3 proved to be the most informative variables for identifying burn scars. The clear visual distinction of burned areas in the principal components suggests a strong potential for developing semi-automated mapping techniques.

A key strength of this multi-temporal approach lies in the ability to detect changes over time, which provides not only the basis for burn scar identification but also insight into their development and eventual recovery patterns. The simple fact of having this capability places great value on fire management and studies in ecology within the fire-prone Mediterranean landscapes.

However, our results indicated that while this methodology of multi-temporal PCA is appropriate for mapping recent burn scars, it overestimates the extent of older burns. This trend of overestimation when the age of fire is rising is an area for future refinement.

This limitation could be overcome by future research investigating the integration of other high-resolution data sources, such as multispectral imagery and LiDAR, for the clear separation of direct fire impacts from the rest of the secondary landscape changes. In this regard, developing methods for accounting for the very rapid vegetation recovery characteristic of Mediterranean ecosystems could save much room for improving the historical mapping of burn scars.

Future directions in research may concern the integration of LiDAR data to capture changes in three-dimensional forest structure post-fire, or hyperspectral imagery sensitive to subtle spectral changes associated with various burn severities. Machine learning techniques might also be explored that allow for the automated discrimination of burn scars from other spectrally similar land cover changes.

Results have important practical implications for forest management. The possibility of mapping recent burn scars could facilitate rapid assessment of fire damage and inform immediate post-fire restoration. Long-term monitoring of ecosystem recovery, informed by the multi-temporal aspect of our approach, should also help managers target areas that might require intervention to promote regeneration. Additionally, historical mapping of burn scars-although currently limited-could provide insight into the fire regimes and improve fire risk models, key to proactive fire management strategies in Mediterranean ecosystems.

References

Atalay, I., Efe, R., Öztürk, M. (2014). Ecology and Classification of Forests in Turkey. *Procedia - Social and Behavioral Sciences,* 120, 788-805. doi.org/10.1016/ J.Sbspro.2014.02.163

Baillarin, S. J., Meygret, A., Dechoz, C., Petrucci, B., Lacherade, S., Tremas, T., Isola, C., Martimort, P., Spoto, F. (2012). Sentinel-2 Level 1 Products and Image Processing Performances. *The International Archives of the Photogrammetry, Remote Sensing and Spatial Information Sciences,* XXXIX-B1, 197–202. doi.org/10.5194/Isprsarchives-XXXIX-B1-197-2012

Bastarrika, A., Chuvieco, E., Martín, M. P. (2011). Mapping Burned Areas from Landsat TM/ETM+ Data with a Two-Phase Algorithm: Balancing Omission and Commission Errors. *Remote Sensing of Environment,* 115(4), 1003-1012, doi.org/10.1016/J.Rse. 2010.12.005

Carper, W. J., Lillesand, T. M., Kiefer, R. W. (1990). The Use of Intensity-Hue-Saturation Transformations for Merging Spot Panchromatic and Multispectral Image Data. *Photogrammetric Engineering Remote Sensing,* 56(4), 459-467.

Choi, M. (2006). A New Intensity-Hue-Saturation Fusion Approach to Image Fusion with a Tradeoff Parameter. *IEEE Transactions on Geoscience and Remote Sensing,* 44(6), 672–1682.

Chu, T., Guo, X. (2013). Remote Sensing Techniques in Monitoring Post-Fire Effects and Patterns of Forest Recovery in Boreal Forest Regions: A Review. In Remote Sensing 6(1), 470-520. doi.org.10.3390/Rs6010470

Chuvieco, E., Martín, M. P., Palacios, A. (2002). Assessment of Different Spectral Indices in the Red-Near-Infrared Spectral Domain For Burned Land Discrimination. *International Journal of Remote Sensing,* 23(23), 5103-5110.

Chuvieco, E., Mouillot, F., Van Der Werf, G. R., San Miguel, J., Tanasse, M., Koutsias, N., García, M., Yebra, M., Padilla, M., Gitas, I., Heil, A., Hawbaker, T. J., Giglio, L. (2019). Historical Background and Current Developments for Mapping Burned Area from Satellite Earth Observation. *Remote Sensing of Environment,* 225, 45-64.

Cihlar, J., Xiao, Q., Chen, J., Beaubien, J., Fung, K., Latifovic, R. (1998). Classification by Progressive Generalization: A New Automated Methodology for Remote Sensing Multichannel Data. *International Journal of Remote Sensing,* 19(14), 2685-2704. doi.org.10.1080/014311698214451

Congalton, R. G. (2015). Remote Sensing and Image Interpretation. 7th Edition. *Photogrammetric*

Engineering Remote Sensing, 81(8). doi.org/ 10.14358/Pers.81.8.615

Congalton, R. G., Green, K. (2008). *Assessing the Accuracy of Remotely Sensed Data: Principles and Practices, Second Edition. In Assessing the Accuracy of Remotely Sensed Data: Principles and Practices,* Second Edition.

Delegido, J., Verrelst, J., Alonso, L., Moreno, J. (2011). Evaluation of Sentinel-2 Red-Edge Bands for Empirical Estimation of Green Lai and Chlorophyll Content. *Sensors,* 11(7), 89-108.

Díaz-Delgado, R., Lloret, F., Pons, X., Terradas, J. (2002). Satellite Evidence of Decreasing Resilience in Mediterranean Plant Communities after Recurrent Wildfires. *Ecology,* 83(8):2293-2303

Fernández-García, V., Marcos, E., Huerta, S., Calvo, L. (2021). Soil-Vegetation Relationships in Mediterranean Forests after Fire. *Forest Ecosystems,* 8(2), 18.

Foody, G. (2010). Assessing the Accuracy of Remotely Sensed Data: Principles and Practices. *The Photogrammetric Record,* 25(130). 9780429143977

Foody, G. M. (2002). Status of Land Cover Classification Accuracy Assessment. *In Remote Sensing of Environment* 80(1), 185-201. doi.org/10.1016/S0034-4257 (01)00295-4

General Directorate of Forestry. (2020). *2020's Statistics in Forestry. Republic of Turkey Ministry of Agriculture and Forestry.*

General Directorate of Forestry. (2022). *2022's Statistics in Forestry.*

Gigović, L., Pourghasemi, H. R., Drobnjak, S., Bai, S. (2019). Testing a New Ensemble Model Based on Svm and Random Forest in Forest Fire Susceptibility Assessment and Its Mapping in Serbia's Tara National Park. *Forests*, 10(5), 408.

Hotelling, H. (1933). Analysis of a Complex of Statistical Variables into Principal Components. *Journal of Educational Psychology,* 24, 417-441.

Huang, D., Jiang, F., Li, K., Tong, G., Zhou, G. (2022). Scaled PCA: A New Approach to Dimension Reduction. *Management Science,* 68(3). doi.org/10.1287/ Mnsc.2021.4020

Kavgacı, A., Başararan, E.A. (2023). *Orman Yangınları*

Key, C. H., Benson, N. C. (2006). Landscape Assessment (La) Sampling and Analysis Methods. In Usda Forest Service - General Technical Report Rmrs-Gtr (Issues 164 Rmrs-Gtr).

Khorrami, B., Gunduz, O., Patel, N., Ghouzlane, S., Najar, M. (2019). Land Surface Temperature Anomalies In Response To Changes In Forest Cover. *International Journal of Engineering and Geosciences,* 4(3). doi.org/10.26833/Ijeg.549944

Lanorte, A., Manzi, T., Nolè, G., Lasaponara, R. (2015). On The Use of the Principal Component Analysis (PCA) For Evaluating Vegetation Anomalies from Landsat-TM NDVI Temporal Series in The Basilicata Region (Italy). *Lecture Notes in Computer Science (Including Subseries Lecture Notes in Artificial Intelligence and Lecture Notes in Bioinformatics),* 9158. doi.org.10.1007/978-3-319-21410-8_16

Lasaponara, R. (2006). On The Use of Principal Component Analysis (PCA) For Evaluating Interannual Vegetation Anomalies from Spot/Vegetation NDVI Temporal Series. Ecological Modelling, 194(4). doi.org.10.1016/J.Ecolmodel. 2005.10.035

Lentile, L. B., Holden, Z. A., Smith, A. M. S., Falkowski, M. J., Hudak, A. T., Morgan, P., Lewis, S. A., Gessler, P. E., Benson, N. C. (2006). Remote Sensing Techniques to Assess Active Fire Characteristics and Post-Fire Effects. *In International Journal of Wildland Fire* (Vol. 15, Issue 3). doi.org.10.1071/Wf05097

Lentile, L. B., Holden, Z. A., Smith, A. M., Falkowski, M. J., Hudak, A. T., Morgan, P., Others, Benson, N. C. (2006). Remote Sensing Techniques to Assess Active Fire Characteristics and Post-Fire Effects. International *Journal of Wildland Fire,* 15(3), 319–345.

Leung, Y., Liu, J., Zhang, J. (2014). An Improved Adaptive Intensity-Hue-Saturation Method for the Fusion Of Remote Sensing Images. *IEEE Geoscience and Remote Sensing Letters,* 11(5). Doi.org.10.1109/Lgrs.2013.2284282

Lillesand, T. M., Kiefer, R. W. (1994). Remote Sensing and Image Interpretation. 3rd Edition. Remote Sensing and Image Interpretation. 3rd Edition.

Liu, S., Zheng, Y., Dalponte, M., Tong, X. (2020). A Novel Fire Index-Based Burned Area Change Detection Approach Using Landsat-8 OLI Data. *European Journal of Remote Sensing,* 53(1), 104-112. doi.org. 10.1080/22797254.2020.1738900

Lu, S. L., Zou, L. J., Shen, X. H., Wu, W. Y., Zhang, W. (2011). Multi-Spectral Remote Sensing Image Enhancement Method Based On PCA and IHS Transformations. Journal of Zhejiang University: Science A, 12(6), 453-460, doi.org.10.1631/ Jzus.A1000282

Lutes, D. C., Keane, R. E., Caratti, J. F., Key, C. H., Benson, N. C., Gang, L. J. (2006). Firemon: Fire Effects Monitoring and Inventory System. *USA Forest Service, Rocky Mountain Research Station, General Technical Report.*

Mallinis, G., Koutsias, N. (2012). Comparing Ten Classification Methods for Burned Area Mapping in a Mediterranean Environment Using Landsat TM Satellite Data. *International Journal of Remote Sensing,* 33(14), 4408-4433 doi.org.10.1080/ 01431161.2011.648284

Mandanici, E., Bitelli, G. (2016). Preliminary Comparison of Sentinel-2 and Landsat 8 Imagery for a Combined Use. *Remote Sensing* 8(12), 1014, 1-9.

Petropoulos, G. P., Kontoes, C., Keramitsoglou, I. (2011). Burnt Area Delineation from A Uni-Temporal Perspective Based On Landsat TM Imagery Classification Using Support Vector Machines. *International Journal of Applied Earth Observation and Geoinformation,* 13(1), 70-80.

Richards, J. A. (2013). Remote Sensing Digital Image Analysis: An Introduction. In Remote Sensing Digital Image Analysis: *An Introduction (Vol. 9783642300622).* doi.org.10.1007/978-3-642-30062-2

Richards, J. A., Jia, X. (2006). *Remote Sensing Digital Image Analysis: An Introduction. In Remote Sensing Digital Image Analysis: An Introduction.* doi.org.10.1007/3-540-29711-1

Röder, A., Hill, J., Duguy, B., Alloza, J. A., Vallejo, R. (2008). Using Long Time Series of Landsat Data to Monitor Fire Events and Post-Fire Dynamics and Identify Driving Factors. A Case Study in the Ayora Region (Eastern Spain). *Remote Sensing of Environment,* 112(1), 259-273. doi.org.10.1016/J.Rse. 2007.05.001

Roteta, E., Bastarrika, A., Padilla, M., Storm, T., Chuvieco, E. (2019). Development of a Sentinel-2 Burned Area Algorithm: Generation of a Small Fire Database For Sub-Saharan Africa. *Remote Sensing of Environment,* 222, 1-17. doi.org.10.1016/J.Rse.2018.12.011

Sabuncu, A., Özener, H. (2019). Uzaktan Algılama Teknikleri ile Yanmış Alanların Tespiti: İzmir Seferihisar Orman Yangını Örneği. *Doğal Afetler Ve Çevre Dergisi*, 5(2), 317-326. doi.org/ 10.21324/dacd.511688

San-Miguel-Ayanz, J., Durrant, T., Boca, R., Libertà, G., Branco, A., De Rigo, D., Ferrari, D., Maianti, P., Artes Vivancos, T., Costa, H., Lana, F. (2020). Advance Effis Report On Forest Fires in Europe, Middle East and North Africa 2019. *In Joint Research Center EC (Issue March).*

Sentinel-2 Mission Overview. (2015). ESA. www.esa.int/

Singh, A., Harrison, A. (1985). Standardized Principal Components. *International Journal of Remote Sensing,* 6(6), 883-896. doi.org.10.1080/01431168508948511

Sunar Erbek, F., Özkan, C., Taberner, M. (2004). Comparison of Maximum Likelihood Classification Method with Supervised Artificial Neural Network Algorithms for Land Use Activities. *International Journal of Remote Sensing,* 25(9), 1733-1748. doi.org.10.1080/0143116031000150077

Tucker, C. J. (1979). Red and Photographic Infrared Linear Combinations for Monitoring Vegetation. *Remote Sensing of Environment,* 8(2), 127-150. doi.org.10.1016/0034-4257 (79) 90013-0

Tuia, D., Volpi, M., Copa, L., Kanevski, M., Muñoz-Marí, J. (2011). A Survey of Active Learning Algorithms for Supervised Remote Sensing Image Classification. *IEEE Journal On Selected Topics in Signal Processing,* 5(3), 606-617. doi.org.10.1109/Jstsp.2011.2139193

Veraverbeke, S., Lhermitte, S., Verstraeten, W. W., Goossens, R. (2011). Evaluation of Pre/Post-Fire Differenced Spectral Indices for Assessing Burn Severity in A Mediterranean Environment with Landsat Thematic Mapper. *International Journal of Remote Sensing,* 32(12), 3521-3537. doi.org.10.1080/ 01431161003752430

Veraverbeke, S., Lhermitte, S., Verstraeten, W., Goossens, R. (2010). *Assessing Burn Severity Using Satellite Time Series. Wit Transactions on Ecology and The Environment,* 137. doi.org.10.2495/Fiva100101

Walsh, S. J., Cooper, J. W., Von Essen, I. E., Gallager, K. R. (1990). Image Enhancement of Landsat Thematic Mapper Data and GIS Data Integration for Evaluation of Resource Characteristics. *Photogrammetric Engineering Remote Sensing*. 56(8), 162-175

Wintz, P. A. (1973). Information Ex. traction, Snr Improvement, And Data Compression in Multispectral Imagery. *IEEE Transactions On Communications,* 21(10), 1121-1131. doi.org.10.1109/Tcom. 1973.1091550